Stall-Induced Vibrations of the AVATAR Rotor Blade

Stall-Induced Vibrations of the AVATAR Rotor Blade

M Stettner, M J Reijerkerk[1], A Lünenschloß[2], V Riziotis[3], A Croce, L Sartori, R Riva[4], J M Peeringa[5]

[1] GE Global Research, Freisinger Landstrasse 50, 85748 Garching, Germany
[2] GE Wind Energy GmbH, Holsterfeld 16, 48499 Salzbergen, Germany
[3] NTUA, P.O. Box 64070, 15710 Zografou, Athens, Greece
[4] Politecnico di Milano, Via La Masa 34, 20156 Milano, Italy
[5] ECN, Westerduinweg 3, 1755 LE Petten, The Netherlands

E-mail: stettner@ge.com

Abstract. In the course of the AVATAR project, partner predictions for key load components in storm/idle conditions separated in two groups. One group showed large loading due to edgewise instability, the other group damped edgewise oscillation and lower load levels. To identify the cause for this separation, the impact of structural and aerodynamic modeling options on damping of stall-induced vibrations is investigated for two simplified operating conditions of a single AVATAR blade. The choice of the dynamic stall model is found to be the primary driver, and is therefore most likely also the reason for previously observed differences in AVATAR storm load predictions. Differences in structural dynamics, mode shapes, structural and dynamic twist, as well as wake model are only secondary in terms of impact on damping. Resolution suffered from failure of system identification methods to extract reliable damping values from various non-linear response simulations.

1. Introduction

Future, very large wind turbines are expected to operate in flow regimes for which current aerodynamic tools lack proper validation. The aim of the EU FP7 project AVATAR (AdVanced Aerodynamic Tools for lArge Rotors) is to improve and validate aerodynamic models and to ensure applicability of aerodynamic models for 10MW+ wind turbines. The project uses a low induction, increased rotor diameter variant of the DTU 10MW reference wind turbine as an aerodynamically challenging vehicle for tool improvement and validation [1].

In the course of the project, several partners assessed system stability in storm load cases and normal operation of the AVATAR research wind turbine [1]. Some simulation results disagreed significantly. For instance, in one group of predictions, blade loads in storm, DLC6.2, exceeded by far loads from other design load cases, DLCs, whereas in a second group all DLCs resulted in comparable, low load levels. This disagreement occurred both for the AVATAR and the INNWIND blade. Simulation methods used for the first set of results predicted an instability in storm, identified as a stall induced vibration, which did not occur with the second set of tools.

In order to identify root causes, researchers of five AVATAR consortium members drilled down on differences in methods and results in a focused study. The present document reviews previous research on the subject, describes the approach taken to identify drivers for the observed disagreement, and presents numerical results quantifying key effects on the AVATAR blade.

2. Review

2.1. Typical section in quasi-steady, detached flow: Impact of polar characteristics

Petersen et al. [2] used quasi-steady, sectional aerodynamics to derive basic relations for in-plane, out-of-plane, and coupling terms of the linearized damping matrix in terms of local in-plane and out-of-plane velocities experienced by the airfoil. The respective damping terms are proportional to sectional chord, air density, and absolute relative velocity, and an expression containing the steady polar lift and drag coefficients, as well their derivative with respect to angle of attack. Hansen [3] introduced instead the mean inflow angle and effective direction of vibration of an elliptical airfoil motion, highlighting the significance of the difference between flapwise and edgewise directions of motion for damping. By separation into terms dependent and independent of the direction of motion, the expressions permit general statements about the impact of airfoil polar characteristics on aerodynamic damping. Damping expressions were derived for a simplified wind turbine system, and suggestions given for tuning of blade modes in order to mitigate instabilities. This approach was expanded later by depicting the combined impact of polar characteristics and direction of motion in a transparent, graphical fashion [4]. The impact of characteristics of the airfoil's polar and its principal directions of motion on aerodynamic damping, based on quasi-steady aerodynamics, can be summarized as follows:

- *Proportionality* – quasi-steady aerodynamic damping is proportional to sectional chord, air density, absolute relative velocity ([2], [5]), and mass ratio, $R_f = \rho c/m_{blade}$, with air density, ρ, chord, c, and blade mass per unit length, m_{blade}.[6].
- *Airfoil polar* – the largest (most positive) overall aero damping occurs in attached flow near angles of attack of 0° or 180° [5], the former being typical for operation in the variable speed region; the lowest aero damping occurs at angles of attack at and above the maximum lift coefficient, C_{Lmax}, for instance on stall regulated machines above rated speed (Fig. 12 of [3]). Petersen et al. [2] generally suggest the use of "soft stall airfoils" with low C_{Lmax}, shallow decline of C_L at angles of attack above C_{Lmax}, and rapid rise of drag coefficient, C_D, at low angles of attack, in order to mitigate stall-induced oscillations.
- *Direction of motion* – aerodynamic damping of blade motion perpendicular to the inflow increases with increasing (positive) lift curve slope [4]. Aerodynamic damping of blade motion in-line with the inflow is generally smaller than damping of out-of-plane oscillation, increases proportionally to drag, and decreases proportionally to lift, drag gradient, $C_{D\alpha}$ ([3], [6]), and lift gradient, $C_{L\alpha}$ ([3], at small inflow angles).

These findings highlight the significance of correct polar data on stability of stall-induced vibrations. With very few exceptions though, steady polar data, either from experiment or simulation, are not available in the critical stall regime. Lennie et al. [7] reviewed extrapolation and correction methods, showing that deviations in predicted polars may account for more than 100% variation in accumulated fatigue damage.

2.2. Blade in two-dimensional quasi-steady, detached flow (strip theory): Impact of structural factors

Expanding on the previous elaborations on exclusively 2D conditions, Petersen et al. [2] investigated the impact of coupling multiple structural sections by means of wind turbine rotor blade modes, still retaining 2D, quasi-steady aerodynamics:

- *Proportionality* – the modal damping ratio is proportional to chord, air density, and absolute velocity (see above for quasi-steady aerodynamic damping), and inversely proportional to the square root of the product of modal mass and modal stiffness. Petersen et al. proposed to increase edgewise stiffness, "even at the expense of added weight" [2].
- *Direction of motion* – Petersen et al. identified increased aerodynamic damping of edgewise modes in normal operation when applying negative structural pitch, that is, inclination of the edgewise motion with respect to the main inflow direction such that the section is at the same time (a) at its maximum deflection towards its leading edge and (b) at its maximum deflection

towards the pressure side. For deep stall around 90° angle of attack, Voutsinas et al. [6] showed that negative (positive) structural pitch shifts the damping minimum towards lower (higher) angles of attack, but has minor impact on the value of the damping minimum itself.

- *Torsion* – (or "dynamic pitch") reduces damping of the first edgewise bending mode if torsion lags bending/edgewise deflection, with minimum damping at 90° phase lag (where torsion towards maximum angle of attack occurs simultaneously with maximum velocity in chordwise direction towards the trailing edge) [2]. Kallesøe [8] showed that bending of the blade under steady-state loading may result in such phased edge-torsion motion.

2.3. Unsteady sectional aerodynamics: Impact of dynamic separation and vortex shedding

The dynamics of blade/airfoil motions inserts unsteadiness into the airflow which is represented by dynamic stall models. These models superimpose a hysteresis loop onto steady airfoil polar characteristics, effectively resulting in a lagging of loads with regard to motion. Dynamic stall models are a standard feature of system level load simulations tools; no single model compares generally more favorably with experimental data than others [9].

While devised for and tuned to flow physics associated with unsteadiness in flow separation (vorticity shedding, separation point motion, leading edge vortex travel), dynamic stall models may also be active and valid in deep stall [9]. Hansen [10] derived a stochastic model specifically for self-induced turbulence in deep stall, tuned to CFD results, and applied it to a typical section using quasi-steady aerodynamics at 90° angle of attack. Addition of stochastic inflow velocities from this model had little impact on the direction of motion at the bifurcation (flutter) point though. Skrzypiński et al. [11] investigated vortex shedding from leading and trailing edge of a typical wind turbine airfoil at 90° angle of attack as a function of non-dimensional edgewise displacement amplitude, A*, and time period, T*, using RANS and LES simulations. "Locking in" of vortex shedding into edgewise airfoil motion occurred near a Strouhal number of 0.13, with the lock-in frequency range widening with growing ratio of airfoil displacement velocity to inflow velocity (as represented by the ratio, A*/T* [11]). At the same time, the peak non-dimensional power extracted from the flow at lock-in was reduced with increasing A*/T*, highlighting the non-linearity of the phenomenon. Voutsinas et al. [6] observed lock-in of drag at twice the lock-in frequency of lift, using a 2D free vortex wake model; due to strongly non-linear behavior, they consider determination of (linear) damping challenging.

The current review did not reveal BEM compatible, computationally efficient, readily applicable, and validated methods addressing vortex shedding on a rotor blade in deep stall.

2.4. Interaction between sections: Wake modelling and three-dimensional coherent structures

BEM-based methods generally exclude spanwise aerodynamic interaction between rotor blade sections, but spanwise flow effects can be included using corrected airfoil polars. Correcting (reducing) the 2D drag coefficient for 3D effects may result in edgewise instability of an individual section [6]. Since spanwise flow is only relevant at root sections, this has little impact on blade stability.

By comparing BEM with CFD and free wake codes, Pirrung et al. [12] showed that neglecting dynamically trailed (near wake) vorticity – as done in classical BEM – may lead to overestimation of the absolute value of aerodynamic work in edgewise oscillations (i.e. when including trailed vorticity, there is less damping in stable, and less excitation in unstable conditions). Interaction between trailing and shed vorticity results in coherent structures which further complicate the situation. Manolesos et al. [13] observed experimentally that such stall cells "... are unstable, display no discernable periodicity, and seem to change position arbitrarily in the spanwise direction". Heinz et al. [14] used CFD to investigate the interaction of coherent structures with elastic wind turbine blades in deep stall. Their results indicate that inclination of the blade with respect to the free stream velocity might correlate the individual sections' shedding frequencies.

Rather than using time-consuming CFD directly, Bertagnolio et al. [15] developed a data-driven grey box approach, using a random process model matched to experimental and DES simulation data.

The model addresses shedding of stochastic and coherent structures from leading and trailing edge of an entire blade, includes coherence between different angles of attack and radial stations, and captures energy peaks from coherent vortex shedding. However, frequencies associated with the energy peaks are overestimated, energy levels in lift and drag are underestimated, and the method cannot capture multiple spanwise stall cells observed in experiments [15]. The authors conclude that the underlying assumption of Gaussian distribution "[…] may underestimate the dynamic load effects" [16].

Consideration of spanwise unsteady aerodynamic interaction between sections, and dissipation of three-dimensional coherent structures in deep stall is subject of ongoing research. To the best knowledge of the authors, respective methods are not available for the majority of present BEM – based loads simulation tools.

3. Approach and Methods

In order to address relevant structural and aerodynamic aspects highlighted in the review section – thus potential causes for differences in damping predictions – various methods were available through participants' tools. With reference to the previous two sub-sections, it is essential to note that these tools neither featured methods addressing vortex-induced oscillations, nor did they consider spanwise unsteady aerodynamic interaction between radial sections.

Three major beam theory implementations were used (short-hand notations introduced in italics in this section are also used in the following plots):

- *Euler* – straight, linear Euler-Bernoulli beam finite elements; no torsion in variant *EulerB*.
- *Timoshenko* – engineering bending theory of beams, in which torsional deformation and transverse shear (as for a Timoshenko beam) flexibility as well as dynamic coupling terms for bending and torsion dynamics are included [17].
- *Exact* – fully populated 6x6 stiffness matrix on initially curved and twisted reference axis, geometrically exact beam type finite elements [18].

Only BEM methods were applied, all implementations using Prandtl tip loss factors, but with differences in high induction/turbulent wake state correction, and consideration of dynamic inflow:

- *StripTheory* – wake disabled, no calculation of induction
- *BEMfrozen* – induced velocity fixed at reference operating condition values
- *BEMdyn* – TUDk dynamic inflow model as suggested by Øye [19]
- *BEMequil* – instantaneously reacting equilibrium wake (using an approximation where inductions are not converged in each simulation time step)

Two-dimensional flow about airfoil sections was modelled both as a quasi-steady phenomenon and using dynamic stall models (see also Holierhoek et al. [9] for a comparison):

- *qs* – quasi-steady sectional aerodynamics, dynamic stall model off
- BL – semi-empirical Beddoes-Leishman [20] model, as implemented in AeroDyn [21]
- ONERA – empirical model with "mean airfoil" parameters [22]

Eigenvalue calculations, finally, were performed by participating partners in two distinctly different ways:

- *SysID* – system identification on the time response of the non-linear system. Variants were *SysID1* with external blade tip follower force impulse excitation and system identification with MOESP algorithm applied to blade root moment and tip displacement signals, and *SysID2* employing wind impulse excitation followed by order 8 subspace identification on blade degrees of freedom.
- *Lin* – eigenvalue analysis for a linearized system model, only in combination with *BEMfrozen*.

In order to minimize any potential disagreement from transferring specification data to tool-specific simulation models, the present study reduced the simulation scope to a single AVATAR blade. Resulting limitations on transferability of conclusions to the remaining project, AVATAR wind turbine design, and its dynamic and stability properties were accepted in favor of simplification. Three different conditions were simulated:

- *blade only* – Eigenvalue solution performed for a blade mounted rigidly to a fixed hub at its root, without gravity loads, aerodynamic loads, and structural damping. The objective was to quantify differences in mass, stiffness, frequency, mode shapes, and particular coupling between bending and torsion.
- *blade as wing* – Eigenvalues were obtained for the first edgewise blade bending mode through a wide range of attached/separated/deep stall flow conditions. Compared to *blade only* conditions, aerodynamic loading from homogeneous, constant inflow at 42 m/s wind speed was included in order to mimic the storm load case addressed in [1].
- *rotating blade* – a study similar to *blade as wing*, but with aerodynamic and inertial loading from 25 m/s wind speed and hub/blade rotating at 9.6 RPM, representative of AVATAR rotor conditions at cut-out in order to investigate the impact of resultant sectional inflow speed on unsteady blade loads and stability.

4. Results

4.1. Excluded by Model and Test Definition

Participants used given tabular data for chord and mass vs. radius, identical operating condition definitions, and identical steady airfoil polars (for a fixed $Re = 13 \cdot 10^6$). These parameters, and derived factors like mass ratio, R_f, blade mass and static moment can therefore be excluded as drivers for deviation in damping predictions (differences from integration of mass distribution were verified to be smaller than 0.005%).

4.2. Blade only: Blade structure characterisation

Shared data also included sectional stiffness properties, but stiffness is also affected by the beam theory. The impact on natural frequency is depicted in Figure 1. Increasingly restricting cross-sectional deflections – from *Exact* via *Timoshenko* to *Euler* and finally *EulerB* – shifts the spectrum to higher values, with the increase for the first edge frequency less than 3%. Increasing cross-sectional constraints increases the flap components of the first edgewise bending mode, while its twist component is reduced, Figure 2. Accordingly, structural pitch (for the given coordinates, the arc tangent of negative ratio of flap to edge component) grows and dynamic pitch (twist) shrinks in magnitude, Figure 3 (no explanation was found for negligible flap components predicted by the *Timoshenko* beam model). These trends could explain over-prediction of damping in stall-induced, edgewise vibrations when quasi-steady aerodynamics are used, per outcome of the review as summarized in section 2.2.

4.3. Blade as wing

Comparisons of damping ratio vs blade pitch for this scenario are presented in Figure 4 through Figure 6. Vertical captions indicate the key flow conditions. 90° pitch relates to free stream inflow from the leading edge, decreasing pitch increases angle of attack through separation in positive stall to deep (positive) stall at 0° pitch, and so on. Pitch values between 90° and 180° represent negative angles of attack and negative stall, respectively. At -90° pitch, the blade experiences reverse flow. The legend identifies the combination of analysis components beam theory, wake model, sectional aerodynamics, and eigensolution used to generate the depicted data set, using the short hand notations introduced in section 3.

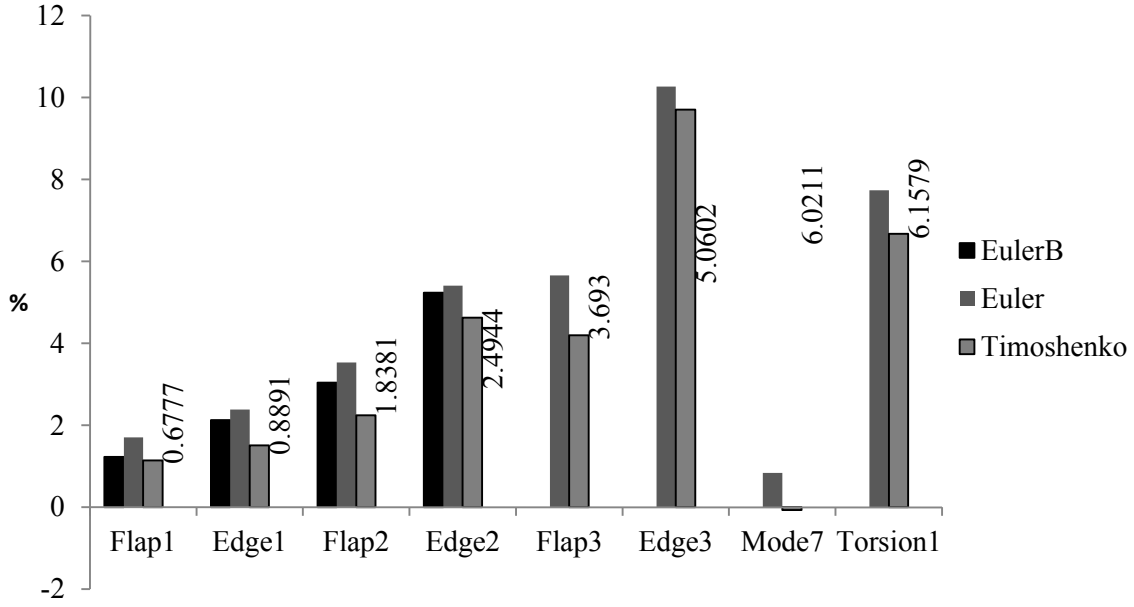

Figure 1: Deviation of blade natural frequency from Exact beam results
(data labels indicate *Exact* beam natural frequency in Hz)

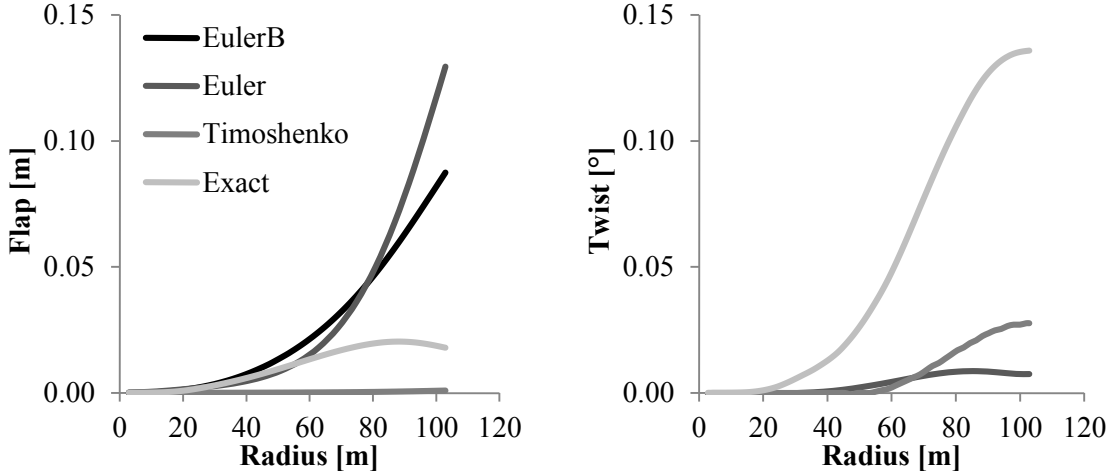

Figure 2: Flap and twist components of edge mode 1, scaled to 1m tip deflection in edge.
flap positive towards suction side, edge positive towards trailing edge, twist positive "nose up"

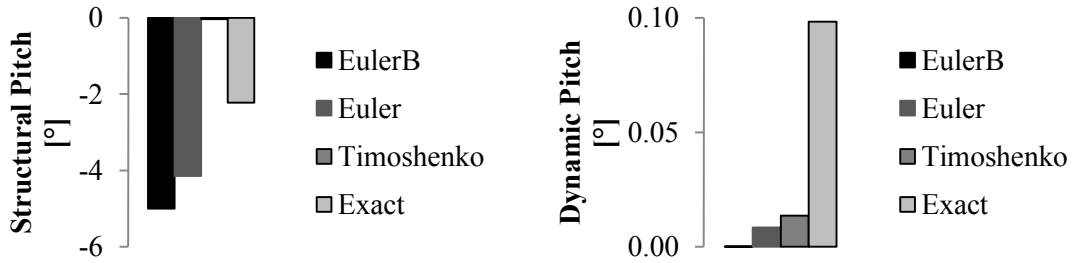

Figure 3: Structural and dynamic pitch of edge mode 1 at 75% rotor radius

Each figure depicts the impact of varying one analysis component at a time, while selecting for the other components the option representing the smallest potential for variation amongst participants' methods (Euler beam, *Euler*, quasi-steady sectional aerodynamics, *qs*, and wake off, *StripTheory*, respectively; exceptions are noted individually).

The vast majority of damping results are above -3%, with damping ratios below -5% in few data points. Since structural damping ratios are frequently set to values between 0.5% and 1.5% [23], instability is present through a wide range of flow conditions except attached flow.

The choice of simple vs. more sophisticated beam models, *Euler/EulerB* vs. *Exact*, respectively, has little effect on stability in the majority of flow conditions when quasi-steady aerodynamics are used, Figure 4. A notable exception is positive stall onset at 70° pitch angle, where only *EulerB* predicts stability. This observation confirms the previously suspected over-prediction of damping by *EulerB* due to its lack of dynamic pitching specifically when quasi-steady sectional aerodynamics are used, see sections 2.2. and 4.2.

However, application of unsteady aerodynamics to *EulerB* removes this feature, Figure 5, and damping in general is significantly increased. *BL* (Beddoes-Leishman) predicts smaller increases than *ONERA*, which even removes instability at all pitch angles but 60°, corresponding to angles of attack around 30°.

Results obtained using *Timoshenko* beam theory indicate damping values in positive stall up to 2% lower than those obtained with other beam theories, Figure 4. Since additional flapwise contributions would insert additional damping, it is suspected that the very small flapwise component observed in the previous section is the main reason for this result. Note that depicted *Timoshenko* results were obtained using including induced velocities provided by *BEMfrozen,* since "wake off" (*StripTheory*) results were not available.

For *EulerB* beam theory, the choice of wake model has little impact on damping, Figure 6.

In conclusion, results indicate that the choice of the dynamic stall model – and its respective, airfoil-dependent parameters – drives stability of the single AVATAR blade in this scenario, and is likely the primary driver for differences in previous AVATAR storm load predictions [1].

4.4. Rotating blade

Results for the rotating blade are presented in Figure 7 through Figure 9 in the same way as for *blade as wing* in the previous section. Inflow conditions are shifted in pitch due to blade rotation, with inflow being aligned with blade tip chord at about 20°, and reverse flow occurring at around -160° pitch. Compared to the *blade as wing* case (with 42 m/s resultant inflow), the following changes are noticeable:

The beam theory has larger impact on damping than in the *blade as wing* scenario, Figure 7; aerodynamic damping in stall decreases consistently with growing restriction in cross sectional deflection.

Aerodynamic damping levels with quasi-steady strip theory dropped from -3% (*blade as wing*) to around -5%, Figure 8. This trend is consistent with growth of magnitude of quasi-steady aerodynamic damping with absolute wind speed, as predicted by e.g. Petersen et al. [2]: Rotating the blade at 9.6RPM in 25 m/s wind leads to 112 m/s resultant inflow velocity at the blade tip, compared to 42 m/s for *blade as wing*. A linear growth in damping is not observed as predicted since only the tip of the rotating blade is exposed to this absolute wind speed. Damping increments due to addition of the Beddoes-Leishman dynamic stall model were nearly unchanged at +2% (compare with Figure 5). *ONERA* still stabilizes the system except at -10° pitch.

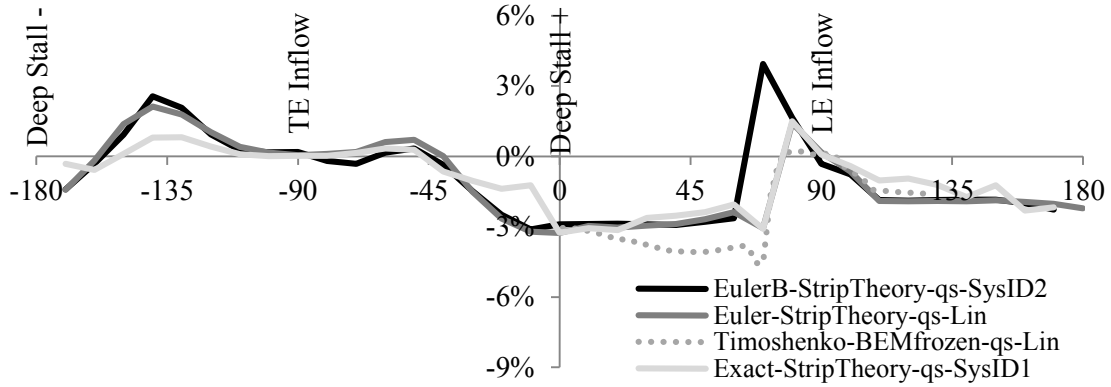

Figure 4: *Blade as wing* edge mode 1 damping ratio [%] vs. pitch [°]:
Beam solutions, quasi-steady section aerodynamics

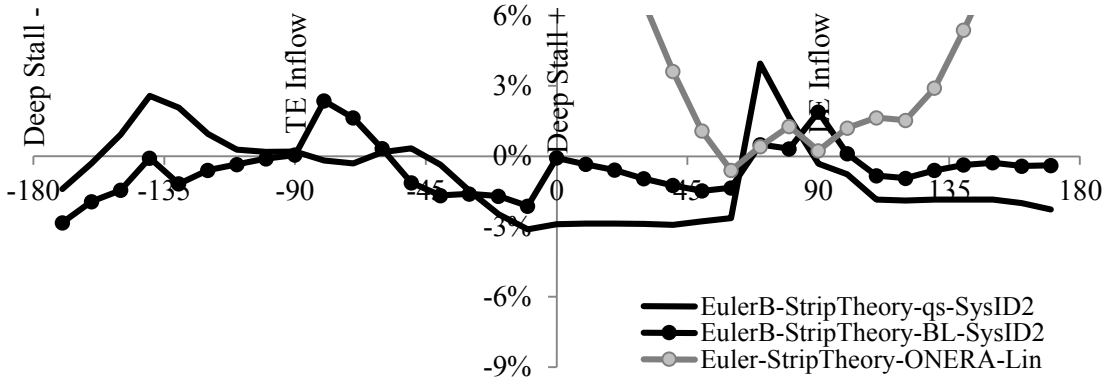

Figure 5: *Blade as wing* edge mode 1 damping ratio [%] vs. pitch [°]:
Section aerodynamics, strip theory (wake off)

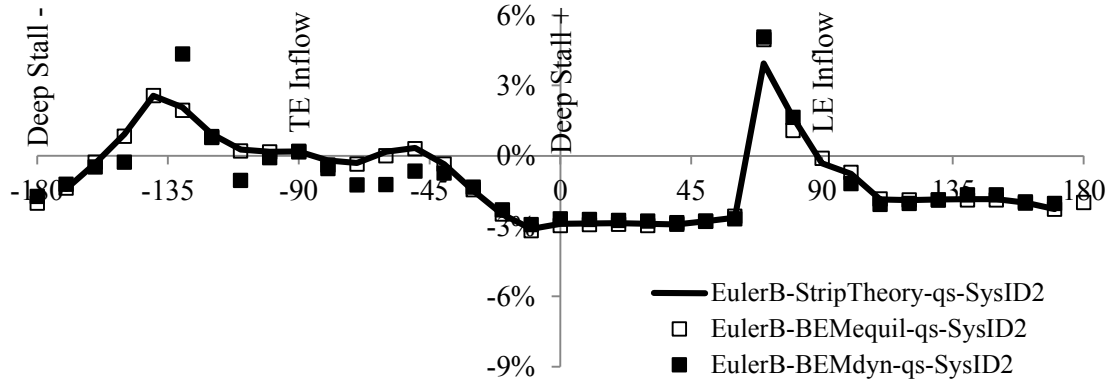

Figure 6: *Blade as wing* edge mode 1 damping [%] vs. pitch [°]:
Wake models, quasi-steady section aerodynamics

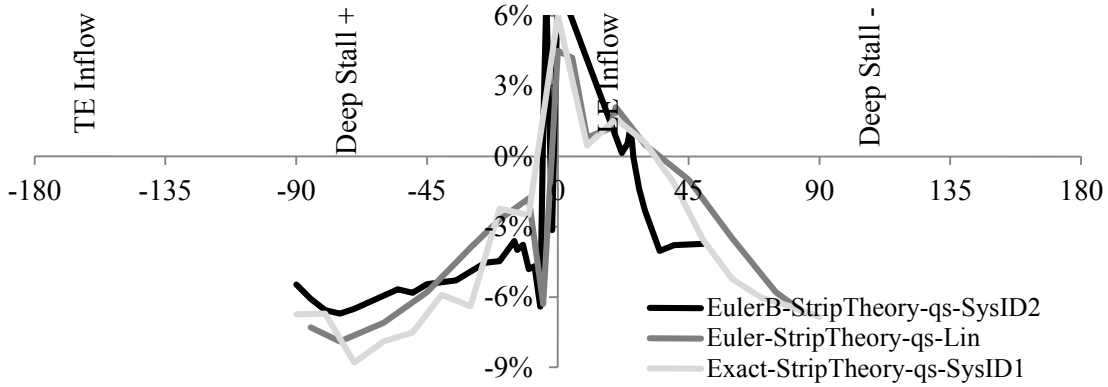

Figure 7: *Rotating blade* edge mode 1 damping ratio [%] vs. pitch [°]:
Beam solutions, quasi-steady section aerodynamics

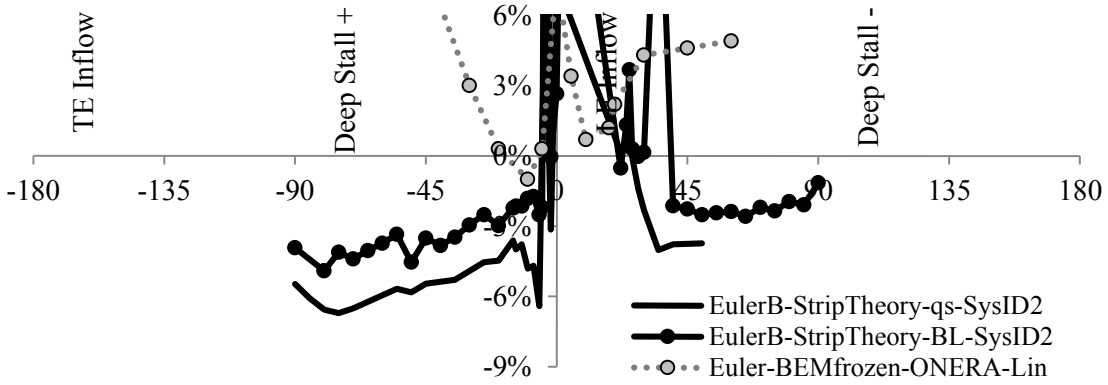

Figure 8: *Rotating blade* edge mode 1 damping ratio [%] vs. pitch [°]:
Section aerodynamics, strip theory (wake off)

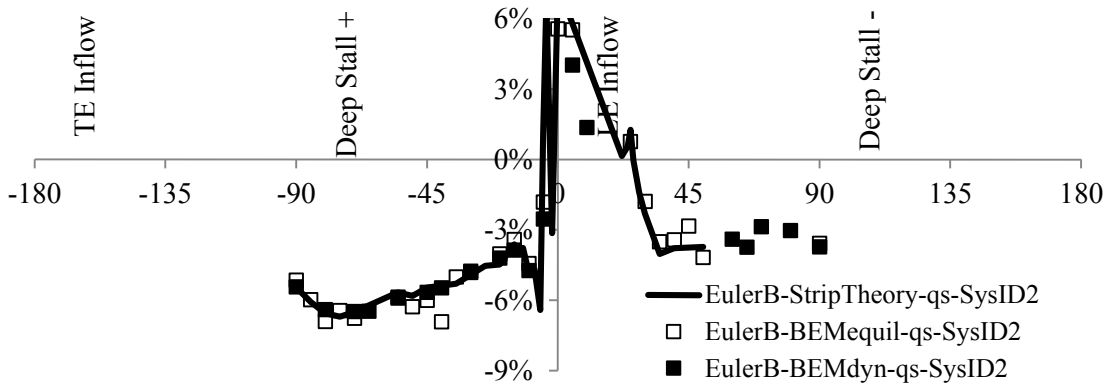

Figure 9: *Rotating blade* edge mode 1 damping [%] vs. pitch [°]:
Wake models, quasi-steady section aerodynamics

In agreement with *blade as wing*, the choice of wake models had little impact generally, and no effect on damping in stall, Figure 9. In case of the dynamic wake, *BEMdyn*, this could certainly be explained by the spectral gap between time scales associated with edgewise vibration, and those relevant for wake dynamics. This explanation does not hold for results with the (quasi-) equilibrium wake, *BEMequil*, which reacts instantaneously to changes in blade loads. Despite high time-averaged loading on the blade, the steady-state and oscillatory pressure load of a single rotor blade appears to be insufficient to generate a significant induced velocity variation.

In attached flow results, differences are mainly attributed to system identification issues which are also apparent in the 50° through 80° pitch range for simulations with quasi-steady aerodynamics. Generally, system identification was found to be sensitive to proper excitation, selection of identification method, and tuning of its parameters, due to non-linearity of the aeroelastic system and complexity of its response. Proper identification and association with physical modes failed in some operating conditions. It is advisable to follow system identification best practice and to complete convergence and tuning studies before extensive application to an unknown dynamic system. Wherever results from linear models are available, these should be used to tune identification algorithms.

5. Conclusions

Results of simulations performed in this investigation show that the choice of the dynamic stall model – and its respective, airfoil-dependent parameters – can make the difference between damped and unstable edgewise oscillation of an individual AVATAR rotor blade. This choice is most likely also the primary driver for differences in early AVATAR storm load predictions. Differences in structural dynamics, mode shapes, and structural and dynamic twist from application of different beam models had only secondary influence on stall-induced vibration damping, albeit being more noticeable in the higher loaded *rotating blade* scenario. In both simplified cases investigated, selection of the wake model had negligible impact. Resolution of results suffered from failure of the applied system identification methods to extract reliable damping results from various non-linear response simulations.

6. Acknowledgements

This project has received funding from the European Union's Seventh Programme for research, technological development and demonstration under grant agreement No FP7-ENERGY-2013-1/no. 608396.

References

[1] Ruiz A I, Madsen H A, Verelst D R, Croce A, Sartori L, Lunghini M S, Reijerkerk M J, Kooijman H, Stettner M 2015 *Comparison of the INNWIND and AVATAR Research Wind Turbines, AVATAR Deliverable D1.3* http://www.eera-avatar.eu/ April 2015

[2] Petersen J T, Madsen H A, Björck A, Enevoldsen P, Øye S, Ganander H, and Winkelaar, D 1998 Prediction of dynamic loads and induced vibrations in stall *Risø-R-1045* (Roskilde, DK: Risø Research Center)

[3] Hansen M H 2003 Improved modal damping of wind turbines to avoid stall-induced vibrations, *Wind Energ.* **6** 179-195

[4] Hansen M H 2007 Aeroelastic instability problems for wind turbines *Wind Energ.* **10** 551-577

[5] Politis E S, Chaviaropoulos P K, Riziotis V A and Voutsinas S G 2009 Stability analysis of parked wind turbine blades *Proc. EWEC 2009*, Marseille

[6] Voutsinas S, Zou F, Riziotis V, and Wang J 2013 Analysis of vortex-induced vibrations using a free-wake aeroelastic tool (presentation) *Proc. EWEA 2013*, Vienna

[7] Lennie M, Pechlivanoglou G, Martin D, Nayeri C N and Paschereit O 2015 A Review of wind turbine polar data and its effect on fatigue loads simulation accuracy *Proc. ASME Turbo Expo 2015*, GT2015-43249 (New York, NY: ASME)

[8] Kallesøe B S 2011 Effect of steady deflections on the aeroelastic stability of a turbine blade *Wind Energ.* **14** 209-224
[9] Holierhoek J G, de Vall J B, van Zuijlen A H and Bijl H 2013 Comparing different dynamic stall models *Wind Energ.* **16** 139-158
[10] Hansen, M H 2009 Bias effect of self-induced turbulence on the stall-flutter limit of an airfoil section *Recent Developments in Acoustics, Noise and Vibration.* Ed Pawelczyk M and Bismor D (Auburn, AL: International Institute of Acoustics and Vibration)
[11] Skrzypiński W, Gaunaa M, Sørensen M, Zahle F, and Heinz J 2014 Vortex-induced vibrations of a DU96-W-180 airfoil at 90° angle of attack *Wind Energ.* **17** 1495-1514
[12] Pirrung G R, Madsen H A and Kim T 2014 The influence of trailed vorticity on flutter speed estimations, The Science of Making Torque from Wind 2014 (TORQUE 2014), *2014 J. Phys.: Conf. Ser.* 524 012048 (Bristol, UK: IOP Publishing)
[13] Manolesos M, Papadakis G and Voutsinas S G. 2014 Experimental and computational analysis of stall cells on rectangular wings *Wind Energ.* **17** 939-955
[14] Heinz J C, Sørensen N N, Zahle F, and Skrzypiński W 2016 Vortex-induced vibrations on a modern wind turbine blade *Wind Energ.* doi: 10.1002/we.1967
[15] Bertagnolio F, Rasmussen F, Sørensen N N, Johansen J and Madsen H A 2008 A stochastic static stall model applied to a wind turbine blade *AIAA 2008-6723* (Washington, DC: AIAA)
[16] Bertagnolio F, Rasmussen F, Sørensen N N, Johansen J and Madsen H A 2010 A stochastic model for the simulation of wind turbine blades in static stall *Wind Energ*. **13** 323-338
[17] Lindenburg C 2003 BLADMODE - Program for rotor blade mode analysis *ECN-C--02-050* (Petten, NL: ECN)
[18] Giavotto V, Borri M, Mantegazza P and Ghiringhelli G 1983 Anisotropic beam theory and applications *Computers & Structures* **16** 403–413
[19] 1995 Joint Investigation of Dynamic Inflow Effects and Implementation of an Engineering Method *ECN-C--94-107* ed Snel H and Schepers J G (Petten, NL: ECN)
[20] Leishman J G and Beddoes T S 1986 A semi-empirical model for dynamic stall *J. American Helicopter Society* **34** 3–17
[21] Moriarty P J and Hansen A C 2004 AeroDyn Theory Manual *NREL/EL-500-36881* (Golden, CO: NREL)
[22] Petot D 1989 Differential Equation Modelling of Dynamic Stall *La Recherche Aérospatiale (English Edition)* pp. 59–72
[23] Jonkman J M and Buhl Jr. M L 2005 FAST User's Guide *NREL/EL-500-29798* (Golden, CO: NREL)